A Closer Look into Two-Step Perovskite Conversion with X-ray Scattering

Johannes Schlipf,[†] Pablo Docampo,[‡] Christoph J. Schaffer,[†] Volker Körstgens,[†] Lorenz Bießmann,[†] Fabian Hanusch,[‡] Nadja Giesbrecht,[‡] Sigrid Bernstorff,[§] Thomas Bein,[‡] and Peter Müller-Buschbaum*[,†]

[†]Lehrstuhl für Funktionelle Materialien, Physik-Department, Technische Universität München, James-Franck-Str. 1, 85748 Garching, Germany

[‡]Department of Chemistry and Center for NanoScience (CeNS), University of Munich (LMU), Butenandtstr. 5-13, 81377 München, Germany

[§]Elettra-Sincrotrone Trieste S.C.p.A., Strada Statale 14 - km 163.5 in AREA SCIENCE PARK, Basovizza, 34149 Trieste, Italy

S *Supporting Information*

ABSTRACT: Recently, hybrid perovskites have gathered much interest as alternative materials for the fabrication of highly efficient and cost-competitive solar cells; however, many questions regarding perovskite crystal formation and deposition methods remain. Here we have applied a two-step protocol where a crystalline PbI_2 precursor film is converted to $MAPbI_{3-x}Cl_x$ perovskite upon immersion in a mixed solution of methylammonium iodide and methylammonium chloride. We have investigated both films with grazing incidence small-angle X-ray scattering to probe the inner film morphology. Our results demonstrate a strong link between lateral crystal sizes in the films before and after conversion, which we attribute to laterally confined crystal growth. Additionally, we observe an accumulation of smaller grains within the bulk in contrast with the surface. Thus, our results help to elucidate the crystallization process of perovskite films deposited via a two-step technique that is crucial for controlled film formation, improved reproducibility, and high photovoltaic performance.
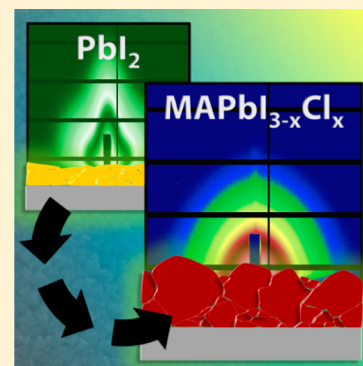
The first application of hybrid organometal halide perovskites as sensitizer in hybrid solar cells by Kojima et al. marks the cornerstone for what has now become a broad field of extensive research.[1] After overcoming initial challenges, power conversion efficiencies (PCE) of hybrid perovskite photovoltaics soon crossed the 10% mark[2] and have steadily risen ever since, now challenging conventional inorganic thin film technologies with ~20% certified PCE.[3,4] The massive interest in this type of material is further nurtured by the easy and versatile processing[5] for improved stability[6] and reproducibility[7] and the abundance of precursor materials, thus rendering hybrid organometal halide perovskites candidates for a low-cost, mass-producible photovoltaic technology.

Having evolved from the conventional dye-sensitized solar-cell architecture incorporating a mesoporous TiO_2 layer, perovskite solar cells are nowadays fashioned in various different designs.[8] Seminal work by Lee et al. and Ball et al. showed that both methylammonium lead iodide perovskite ($MAPbI_3$) and the similar $MAPbI_{3-x}Cl_x$ (with a certain amount of Cl^- present during film formation) exhibit ambipolar charge transport.[2,9] In combination with large charge-carrier diffusion lengths, this allows for omission of the mesoporous scaffold in perovskite solar cells and has led to the introduction of planar p-i-n heterojunction architectures. Several deposition techniques have been developed for this configuration; in particular, a two-step preparation protocol has led to highly efficient devices: Hereby a crystalline lead iodide (PbI_2) precursor

layer is deposited via spin-coating from solution and subsequently converted to a dense perovskite film by immersion into a solution containing methylammonium iodide (MAI).[10,11] Further improvements in terms of photovoltaic performance include the incorporation of methylammonium chloride (MACl) into the conversion step, which enhances the lifetime of photoexcited species generated within the film.[12,13] These advances illustrate that to achieve the highest performing devices it is crucial to optimize film formation, that is, to understand the underlying crystallization process.[14] While a comprehensive understanding of the single-step perovskite deposition process already exists,[15] less attention has been given to the more versatile two-step deposition approach. Recently, various alterations to the basic two-step deposition have been proposed to improve photovoltaic performance and reproducibility of devices.[7,16−22] Many of these advanced protocols focus on the optimization of the PbI_2 precursor layer; however, in-depth knowledge about the formation of the final film morphology is still lacking.[23,24]

In this work, we have prepared $MAPbI_{3-x}Cl_x$ perovskite films via a two-step deposition with a mixed MAI/MACl conversion solution and have performed grazing incidence small-angle X-

ray scattering (GISAXS) experiments on both initial PbI_2 and final perovskite films. Our results show a strong correlation between lateral crystal sizes in both films, proving the importance of optimized PbI_2 deposition for this preparation technique. From this observation, we have developed a tentative model for the conversion process itself and provide a route toward controlled film formation and higher photovoltaic performance.

The films prepared in this work were fabricated according to a previously published protocol that is described in detail in the Supporting Information (SI).[13] In short, a solution of PbI_2 in dimethylformamide (DMF) is spin-cast onto a silicon substrate and the dry film is then immersed into a bath of isopropyl alcohol (IPA) at 60 °C containing 9.5 mg/mL MAI and 0.5 mg/mL MACl. As pointed out previously, a crucial point for achieving homogeneous films and optimized photovoltaic performance is the very fast crystallization of PbI_2 upon spin-coating by keeping both solution and substrate at 60 °C.[13]

To probe the structural properties of the prepared films, both the initial lead iodide layer and the perovskite film were studied with GISAXS. Measurements were conducted at the Austrian SAXS beamline at Elettra-Sinctrotrone Trieste, Italy. GISAXS has been shown to be a powerful tool to probe the nanometer-scale morphology of thin organic and inorganic films and to explain morphological implications for their behavior in organic and dye-sensitized solar cells.[25−27] Thus, GISAXS is complementary to imaging techniques like atomic force microscopy (AFM) or scanning electron microscopy (SEM), which only probe the sample surface. The combination of the high flux of the synchrotron with the large sample area probed in grazing incidence geometry results in good statistics and allows for short measurement times. Thus, the influence of X-rays on the investigated material is minimized, rendering the method nondestructive. At grazing angles close to the critical angle of the material (usually <1°) the beam penetrates the film, while the contribution from the flat substrate is negligible. The diffuse scattering signal is captured by a Pilatus3 1M area detector, and information on the lateral structures of the films is deduced within the framework of the distorted wave Born approximation (DWBA).[28,29] The crystal structures of PbI_2 and perovskite were monitored by simultaneous wide-angle measurements (GIWAXS) with a second detector (Pilatus 100k). For more details of the experimental procedure and data evaluation we refer the reader to literature[27] and the SI.

Figure 1 shows four horizontal line cuts taken at different positions of the 2D GISAXS data for both samples (cf. Figure S1 in the SI): The scattering signal obtained with an incident beam impinging under the critical angle of the material is highly sensitive to the sample surface (Figure 1b), while at larger angles the beam penetrates the film completely and thus yields information on the volume morphology (Figure 1a).[30] We model the scattering signal within the DWBA to fit the data.[25,28] In the graph, this is represented by blue and red curves for the PbI_2 and perovskite film, respectively. The sample−detector distance was selected to investigate smaller structures below the resolution limit of SEM; however, this sets an upper resolution limit for this measurement, and the largest crystals around 0.5 to 1 μm are not accessible.

To investigate the development of differently sized crystals, we assign three form factors to model the curves within the local monodisperse approximation that describes the scattering signal as the superposition of scattering from individual centers of different size: large crystals (FF1) in the range over 100 nm
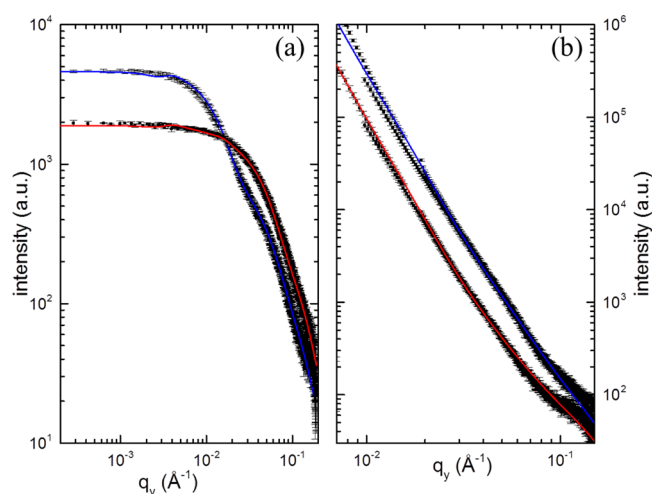

Figure 1. Bulk (a) and surface (b) scattering data of PbI_2 and perovskite films. Black data points belong to horizontal line cuts at a position above the specular peak for a large incident angle (a) and at the Yoneda region with the incident beam impinging at the critical angle (b). Solid lines are the respective model curves fit to the data for PbI_2 (blue) and perovskite (red).

radius, small crystals (FF2) of 20−100 nm, and very small crystals (FF3) of ≤20 nm. Considering radii with a Gaussian size distribution, the model is able to reproduce the scattering signal for the bulk measurements above the beamstop very well, as indicated by the small error bars in Figure 2, where the
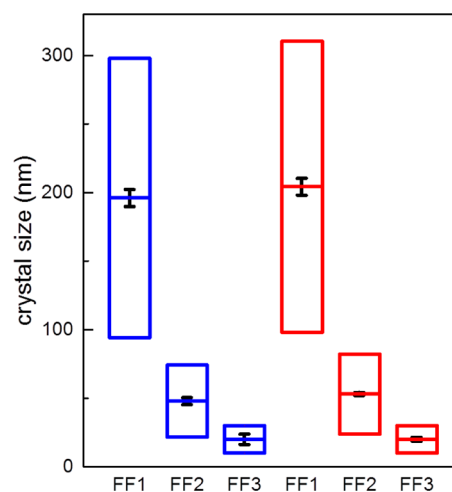

Figure 2. Form factors for PbI_2 (blue) and perovskite (red) extracted from the model curve in Figure 1. Boxes indicate the standard deviation from the mean value with a Gaussian distribution. The small error bars indicate a good validity.

extracted form factors are plotted with their standard deviation (boxes). The color code is the same as above, that is, blue for PbI_2 and red for perovskite. We assign the same radii to model the curves of the surface-sensitive measurements, and although a part of the signal is shielded by the beamstop ($q_y < 10^{-2}$ Å^{-1}) the model curves fit the data well (cf. Figure 1b).

Our results clearly show a striking resemblance of (lateral) crystal sizes in the precursor and the perovskite film, implicating a constrained crystal growth during the conversion step parallel to the substrate (Figure 2). This is remarkable because the PbI_2 unit cell has to expand to include the MA$^+$

PbI$_2$	surface	bulk
small : large	0.8 : 1	10 : 1
small/volume	5.1 %	40 %

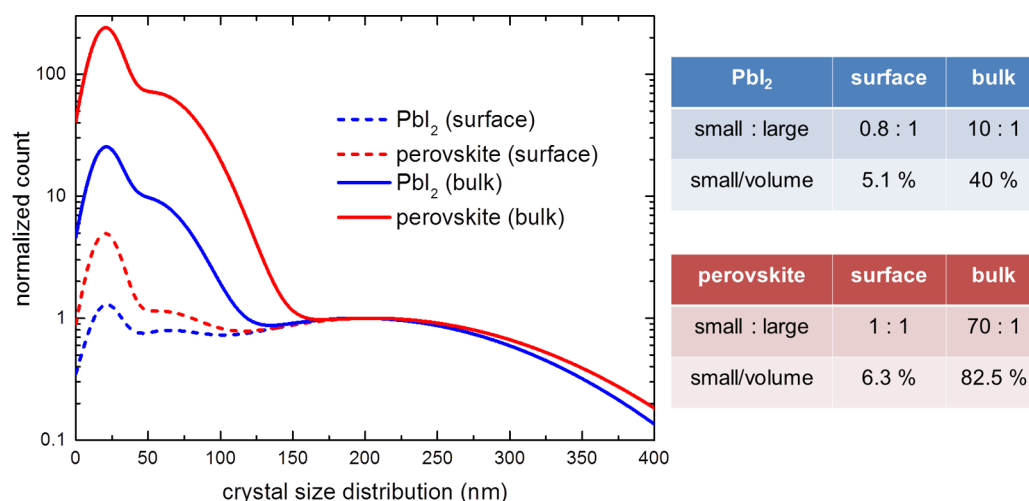| perovskite	surface	bulk
small : large	1 : 1	70 : 1
small/volume	6.3 %	82.5 %

Figure 3. Crystal size distributions are given by the superposition of the Gaussian distributions for the three form factors extracted from the fits and normalized to FF1 (~200 nm). Ratios of small (FF2) to large (FF1) crystals are extracted from peak intensities, and volume fractions of small crystals are estimated.

cations.[31] This leads us to conclude that the dominant crystal growth must take place in the vertical direction, which is supported by previous measurements of increasing film thickness from PbI$_2$ to perovskite,[31,32] yet such anisotropic growth would lead to significant strain within the crystals and cause them to separate into smaller units. The resulting nonuniform vertical distribution of crystal sizes is supported by SEM images of sample cross sections for similar samples (cf. Figure S3 in the SI).

To quantify our findings from GISAXS, we analyze the intensities associated with scattering from individual form factors extracted from the modeling: As intensities scale linearly with the number of crystals of a specific size, the superposition of the Gaussian distributed form factors relates to the crystal size distribution. Figure 3 shows these distributions for each individual fit normalized to the number of large crystals (FF1). Thus, the ratios of small to large crystals (FF2/FF1) are given directly by the peak values. It should be noted that we exclude the smallest objects (FF3) in the following discussion because the background signal arising from film roughness interferes with their intensity values. Ratios of small (FF2) to large (FF1) crystals are given in Figure 3, along with an estimate of the volume ratio. Already in the PbI$_2$ film there is a larger amount of smaller crystals inside the bulk than closer to the film surface. This depletion of smaller crystals with respect to larger ones on the film surface is further supported by SEM images (cf. Figure S3 in the SI). The disparity further increases upon conversion of PbI$_2$ to perovskite, as crystals inside the bulk probably split due to the strain. Smaller crystals on the surface, however, are either detached and washed away in the conversion solution and the subsequent rinsing, or, alternatively, they are partially dissolved and united with the larger crystals by Ostwald-type ripening.[33] The latter process appears to be unlikely due to the low solubility of crystalline PbI$_2$ in IPA; however, smaller crystals on the surface could also react upon strain by epitaxial assimilation, that is, merging with the larger crystals by continuation of their crystal lattice. They cannot do this in the bulk due to spatial constraints and differences in crystal orientations of adjacent domains; however, we do not exclude Ostwald-type ripening in the bulk: Medium-sized crystals would then continue to grow in the same orientation as

adjacent larger ones, while the residues would contribute to the group of smaller crystals in this treatment (FF2 and FF3). To further confirm our findings obtained from modeling with abstract form factors, we complemented the GISAXS study with a careful analysis of powder X-ray diffraction data and found anisotropically strained crystals of similar size as FF2 (cf. Figure S4 in the SI).

Thus, the analysis of the evolution of relative amounts of small and large crystal domains gives insights into the conversion process during the preparation of perovskite films with two-step methods. The observations previously discussed are summarized graphically in Figure 4, which shows the
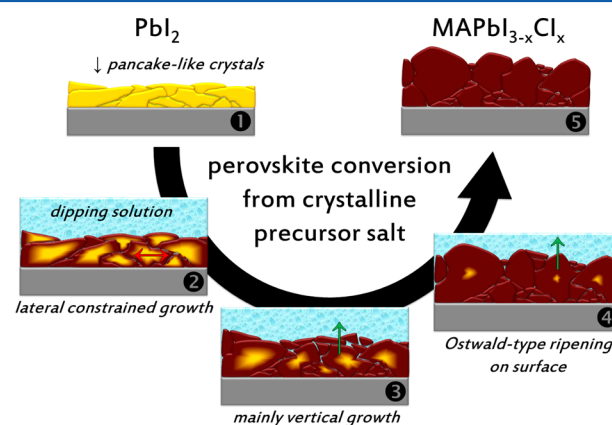

Figure 4. Schematic representation of the proposed mechanism: Because of lateral confinement crystals grow mainly in the vertical direction. The resulting strain inside the film leads to cracking into smaller units, while smaller crystals on the surface grow together.

conversion process combining the information gained from modeling the scattering signal with abstract shapes (form factors) and from a typical film morphology, as seen in cross-sectional SEM images (cf. Figure S3 in the SI). Initially, the precursor film consists of densely packed pancake-like PbI$_2$ crystals layered on top of each other (yellow). Upon immersion into the conversion solution the crystals start to expand as they are converted to MAPbI$_{3-x}$Cl$_x$ perovskite by migration of MA$^+$ cations from the grain boundaries;[31] however, because of the

dense packing their growth is constrained laterally so the dominant growth is in an upward direction. The resulting strain leads to cracking of the crystals, which results in smaller grains being enclosed inside the film; however, on the surface, they contribute to form larger crystals. This description seems to contradict a previous study: Moore et al. suggest a complete reorganization of constituting ions;[15] however, they used a PbCl$_2$ precursor layer, and thus we conclude that whether ionic reorganization takes place might in fact depend on the halide species already contained in the precursor layer. To some extent, iodide seems to be favorable above chloride for incorporation into the perovskite.[34] This may be the reason for the apparent morphological continuation observed in our study where the organic cation is introduced into an already crystalline layer. Considering a recent study, another possibility is that the MA$^+$ ion gradient from the surface to the inner film plays an important role: It could explain why we observe a complete dissolution and recrystallization on the surface (at high concentrations) but topotactic transformation of the crystals in the bulk (low concentrations).[35] In fact, preliminary tests with varying MA$^+$ concentrations in the conversion solution suggest a breakdown of the described mechanism at high concentrations (cf. Figure S5 in the SI).

Understanding the morphology and implied crystal growth processes of two-step perovskite deposition is a major step toward controlling the morphology in other related methods as it marks the starting point for many advanced and more complicated deposition protocols: Some modify the basic protocol investigated here by prewetting of PbI$_2$ with IPA,[16] additional spin-coating and heating steps,[17,18] and solvent post-treatments.[7] Others adapt the principle of two-step deposition but rather rely on sublimating MAI vapor[19,20] or an interdiffusion process by spin-coating the conversion solution onto the PbI$_2$ layer[21] or start from an amorphous PbI$_2$ layer by substituting DMF for dimethyl sulfoxide (DMSO) such that the perovskite is formed from an intermediate complex.[22] Thus, the process described here can serve as a model system to understand conversion processes of a range of two-step methods to help improve them further, which is important because a crystal size gradient in the direction of primary charge transport can have a severe impact on solar cell performance. Controlling the formation of perovskite crystals can help to make perovskite solar cells more reproducible, reduce I–V hysteresis, and lead to high PCE of >20%.[23,24,36]

In conclusion, we conducted GISAXS measurements on a perovskite film and its precursor for a typical and facile method that has been shown before to yield highly efficient perovskite solar cells. Using a model to reproduce the scattering data reveals a close correlation of lateral crystal sizes inside both films. Furthermore, considering the individual scattering intensities of differently sized crystals we deduce an increasing ratio of smaller to larger crystals from the surface to the bulk of the perovskite film. Thus, we also gain insights into the conversion process from PbI$_2$ to MAPbI$_{3-x}$Cl$_x$ perovskite, a protocol that serves as a basis for many other methods. Therefore, its understanding is important for the development and optimization of future preparation protocols and eventually a cost-competitive photovoltaic technology.

ASSOCIATED CONTENT

Ⓢ Supporting Information

2D scattering data for simultaneously conducted small- and wide-angle X-ray scattering experiments, more detailed information on experimental procedures, fit model, and the analysis of particle size ratios, surface and cross-section SEM images, powder X-ray diffraction analysis, and growth mechanism at high concentrations. This material is available free of charge via the Internet at http://pubs.acs.org.

AUTHOR INFORMATION

Corresponding Author

*Tel: +49 (89) 289-12451. E-mail: muellerb@ph.tum.de. Fax: +49 (89) 289-12473.

Notes

The authors declare no competing financial interest.

ACKNOWLEDGMENTS

REFERENCES

(1) Kojima, A.; Teshima, K.; Shirai, Y.; Miyasaka, T. Organometal Halide Perovskites as Visible-Light Sensitizers for Photovoltaic Cells. *J. Am. Chem. Soc.* **2009**, 6050−6051.

(2) Lee, M. M.; Teuscher, J.; Miyasaka, T.; Murakami, T. N.; Snaith, H. J. Efficient Hybrid Solar Cells Based on Meso-Superstructured Organometal Halide Perovskites. *Science* **2012**, 643−647.

(3) Park, N.-G. Perovskite Solar Cells: Switchable Photovoltaics. *Nat. Mater.* **2015**, *14*, 140−141.

(4) Zhou, H.; Chen, Q.; Li, G.; Luo, S.; Song, T.-b.; Duan, H.-S.; Hong, Z.; You, J.; Liu, Y.; Yang, Y. Interface Engineering of Highly Efficient Perovskite Solar Cells. *Science* **2014**, 542−546.

(5) Liu, D.; Kelly, T. L. Perovskite Solar Cells With a Planar Heterojunction Structure Prepared Using Room-Temperature Solution Processing Techniques. *Nat. Photon* **2013**, 133−138.

(6) Law, C.; Miseikis, L.; Dimitrov, S.; Shakya-Tuladhar, P.; Li, X.; Barnes, P. R. F.; Durrant, J.; O'Regan, B. C. Performance and Stability of Lead Perovskite/TiO$_2$, Polymer/PCBM, and Dye Sensitized Solar Cells at Light Intensities up to 70 Suns. *Adv. Mater.* **2014**, 6268−6273.

(7) Bi, D.; El-Zohry, A. M.; Hagfeldt, A.; Boschloo, G. Improved Morphology Control Using a Modified Two-Step Method for Efficient Perovskite Solar Cells. *ACS Appl. Mater. Interfaces* **2014**, 18751−18757.

(8) Snaith, H. J. Perovskites: The Emergence of a New Era for Low-Cost, High-Efficiency Solar Cells. *J. Phys. Chem. Lett.* **2013**, 3623−3630.

(9) Ball, J. M.; Lee, M. M.; Hey, A.; Snaith, H. J. Low-Temperature Processed Meso-Superstructured to Thin-Film Perovskite Solar Cells. *Energy Environ. Sci.* **2013**, 1739.

(10) Liang, K.; Mitzi, D. B.; Prikas, M. T. Synthesis and Characterization of Organic−Inorganic Perovskite Thin Films Prepared Using a Versatile Two-Step Dipping Technique. *Chem. Mater.* **1998**, 403−411.

(11) Burschka, J.; Pellet, N.; Moon, S.-J.; Humphry-Baker, R.; Gao, P.; Nazeeruddin, M. K.; Grätzel, M. Sequential Deposition as a Route to High-Performance Perovskite-Sensitized Solar Cells. *Nature* **2013**, 316−319.

(12) Liu, M.; Johnston, M. B.; Snaith, H. J. Efficient Planar Heterojunction Perovskite Solar Cells by Vapour Deposition. *Nature* **2013**, 395−398.

(13) Docampo, P.; Hanusch, F.; Stranks, S. D.; Döblinger, M.; Feckl, J. M.; Ehrensperger, M.; Minar, N. K.; Johnston, M. B.; Snaith, H. J.;

Bein, T. Solution Deposition-Conversion for Planar Heterojunction Mixed Halide Perovskite Solar Cells. *Adv. Energy Mater.* **2014**, 1400355.

(14) Grancini, G.; Marras, S.; Prato, M.; Giannini, C.; Quarti, C.; Angelis, F. de; Bastiani, M. de; Eperon, G. E.; Snaith, H. J.; Manna, L.; et al. The Impact of the Crystallization Processes on the Structural and Optical Properties of Hybrid Perovskite Films for Photovoltaics. *J. Phys. Chem. Lett.* **2014**, 3836−3842.

(15) Moore, D. T.; Sai, H.; Wee Tan, K.; Estroff, L. A.; Wiesner, U. Impact of the Organic Halide Salt on Final Perovskite Composition for Photovoltaic Applications. *APL Mater.* **2014**, 081802.

(16) Zheng, L.; Ma, Y.; Chu, S.; Wang, S.; Qu, B.; Xiao, L.; Chen, Z.; Gong, Q.; Wu, Z.; Hou, X. Improved Light Absorption and Charge Transport for Perovskite Solar Cells with Rough Interfaces by Sequential Deposition. *Nanoscale* **2014**, 8171.

(17) Shi, J.; Luo, Y.; Wei, H.; Luo, J.; Dong, J.; Lv, S.; Xiao, J.; Xu, Y.; Zhu, L.; Xu, X.; et al. Modified Two-Step Deposition Method for High-Efficiency $TiO_2/CH_3NH_3PbI_3$ Heterojunction Solar Cells. *ACS Appl. Mater. Interfaces* **2014**, 9711−9718.

(18) Xu, Y.; Shi, J.; Lv, S.; Zhu, L.; Dong, J.; Wu, H.; Xiao, Y.; Luo, Y.; Wang, S.; Li, D.; et al. Simple Way to Engineer Metal−Semiconductor Interface for Enhanced Performance of Perovskite Organic Lead Iodide Solar Cells. *ACS Appl. Mater. Interfaces* **2014**, *6* (8), 5651−5656.

(19) Chen, Q.; Zhou, H.; Hong, Z.; Luo, S.; Duan, H.-S.; Wang, H.-H.; Liu, Y.; Li, G.; Yang, Y. Planar Heterojunction Perovskite Solar Cells via Vapor-Assisted Solution Process. *J. Am. Chem. Soc.* **2014**, 622−625.

(20) Hu, H.; Wang, D.; Zhou, Y.; Zhang, J.; Lv, S.; Pang, S.; Chen, X.; Liu, Z.; Padture, N. P.; Cui, G. Vapour-Based Processing of Hole-Conductor-Free $CH_3NH_3PbI_3$ Perovskite/C_{60} Fullerene Planar Solar Cells. *RSC Adv.* **2014**, 28964.

(21) Xiao, Z.; Bi, C.; Shao, Y.; Dong, Q.; Wang, Q.; Yuan, Y.; Wang, C.; Gao, Y.; Huang, J. Efficient, High Yield Perovskite Photovoltaic Devices Grown by Interdiffusion of Solution-Processed Precursor Stacking Layers. *Energy Environ. Sci.* **2014**, 2619.

(22) Wu, Y.; Islam, A.; Yang, X.; Qin, C.; Liu, J.; Zhang, K.; Peng, W.; Han, L. Retarding the Crystallization of PbI_2 for Highly Reproducible Planar-Structured Perovskite Solar Cells via Sequential Deposition. *Energy Environ. Sci.* **2014**, 2934.

(23) Zhao, Y.; Zhu, K. Solution Chemistry Engineering toward High-Efficiency Perovskite Solar Cells. *J. Phys. Chem. Lett.* **2014**, 4175−4186.

(24) Egger, D. A.; Edri, E.; Cahen, D.; Hodes, G. Perovskite Solar Cells: Do We Know What We Do Not Know? *J. Phys. Chem. Lett.* **2015**, 279−282.

(25) Müller-Buschbaum, P. Grazing Incidence Small-Angle X-Ray Scattering: an Advanced Scattering Technique for the Investigation of Nanostructured Polymer Films. *Anal. Bioanal. Chem.* **2003**, 3−10.

(26) Schaffer, C. J.; Palumbiny, C. M.; Niedermeier, M. A.; Jendrzejewski, C.; Santoro, G.; Roth, S. V.; Müller-Buschbaum, P. A Direct Evidence of Morphological Degradation on a Nanometer Scale in Polymer Solar Cells. *Adv. Mater.* **2013**, 6760−6764.

(27) Müller-Buschbaum, P. The Active Layer Morphology of Organic Solar Cells Probed with Grazing Incidence Scattering Techniques. *Adv. Mater.* **2014**, 7692−7709.

(28) Renaud, G.; Lazzari, R.; Leroy, F. Probing Surface and Interface Morphology with Grazing Incidence Small Angle X-Ray Scattering. *Surf. Sci. Rep.* **2009**, 255−380.

(29) Lazzari, R. IsGISAXS: a Program for Grazing-Incidence Small-Angle X-Ray Scattering Analysis of Supported Islands. *J. Appl. Crystallogr.* **2002**, 406−421.

(30) Yoneda, Y. Anomalous Surface Reflection of X Rays. *Phys. Rev.* **1963**, 2010.

(31) Liu, D.; Gangishetty, M. K.; Kelly, T. L. Effect of $CH_3NH_3PbI_3$ Thickness on Device Efficiency in Planar Heterojunction Perovskite Solar Cells. *J. Mater. Chem. A* **2014**, 19873−19881.

(32) Docampo, P.; Hanusch, F. C.; Giesbrecht, N.; Angloher, P.; Ivanova, A.; Bein, T. Influence of the Orientation of Methylammo-nium Lead Iodide Perovskite Crystals on Solar Cell Performance. *APL Mater.* **2014**, 081508.

(33) Ostwald, W. The Formation and Changes of Solids. *Z. Phys. Chem.* **1897**, 289−330.

(34) Colella, S.; Mosconi, E.; Fedeli, P.; Listorti, A.; Gazza, F.; Orlandi, F.; Ferro, P.; Besagni, T.; Rizzo, A.; Calestani, G.; et al. $MAPbI_{3−x}Cl_x$ Mixed Halide Perovskite for Hybrid Solar Cells: The Role of Chloride as Dopant on the Transport and Structural Properties. *Chem. Mater.* **2013**, 4613−4618.

(35) Yang, S.; Zheng, Y. C.; Hou, Y.; Chen, X.; Chen, Y.; Wang, Y.; Zhao, H.; Yang, H. G. Formation Mechanism of Freestanding $CH_3NH_3PbI_3$ Functional Crystals: In Situ Transformation vs Dissolution−Crystallization. *Chem. Mater.* **2014**, 6705−6710.

(36) Kim, H.-S.; Park, N.-G. Parameters Affecting I−V Hysteresis of $CH_3NH_3PbI_3$ Perovskite Solar Cells: Effects of Perovskite Crystal Size and Mesoporous TiO_2 Layer. *J. Phys. Chem. Lett.* **2014**, 2927−2934.